

**HYDROTHERMAL SYNTHESIZED ZINC OXIDE
NANOPARTICLES WITH MANGANESE DOPING
FOR SUPERCAPACITOR**

KIONG YUEN YEE

UNIVERSITI SAINS MALAYSIA

2022

**SCHOOL OF MATERIALS AND MINERAL RESOURCES ENGINEERING
UNIVERSITI SAINS MALAYSIA**

**HYDROTHERMAL SYNTHESIZED ZINC OXIDE NANOPARTICLES WITH
MANGANESE DOPING FOR SUPERCAPACITOR**

By

KIONG YUEN YEE

Supervisor: Assoc. Prof. Dr. Ahmad Azmin Mohamad

**Dissertation submitted in partial fulfillment of the requirements for the degree of
Bachelor of Engineering with Honours
(Materials Engineering)**

Universiti Sains Malaysia

August 2022

DECLARATION

I hereby declare that I have conducted, completed the research work and written the dissertation entitled 'Hydrothermal Synthesized Zinc Oxide Nanoparticles with Manganese Doping for Supercapacitor'. I also declare that it has not been previously submitted for the award of any degree and diploma or other similar title of this for any other examining body or University.

Name of Student: Kiong Yuen Yee

Signature:

Date: 15 August 2022



Witness by

Supervisor: Assoc. Prof. Dr. Ahmad Azmin

Signature:

Mohamad

Date: 15 August 2022



AHMAD AZMIN MOHAMAD
BSc Hons (Malaya), PhD (Malaya), Ceng (MIMechE)
Associate Professor
School of Materials & Mineral Resources Engineering,
Universiti Sains Malaysia,
14300 Nibong Tebal, Penang, Malaysia
Email: aam@usm.com

ACKNOWLEDGEMENTS

First and foremost, I would like to express my deep sense of gratitude to University Sains Malaysia (USM) and School of Materials and Mineral Resources Engineering for providing me opportunity, adequate equipment and to complete this research. A sincerely appreciation goes out to my research supervisor, Associate Prof. Dr. Ahmad Azmin Mohamad for his precious guidance and support throughout this research. His immerse knowledge, dedication, patience and motivation have deeply inspired me and helped me to a very great extent in completing this research. I also want to thank him for willing to share his experience through presentations and advices.

Besides, I am also highly grateful to Ms. Nor Azmira Binti Salleh @ Ramlee for her assistance and dedicated involvement in every stage of this study especially led me in proper handling of experimental equipment and materials. I appreciated her willingness to share her knowledges and offer useful suggestions.

On top of that, I would like to that this would chance to extend my deepest respect all the technicians and supporting staffs especially Puan Haslina, Encik Mohd Azam, Encik Abd Rashid, Encik Muhammad Azrul and Encik Meor Mohamad Noh from School of Materials and Mineral Resources Engineering; Encik Muhammad Fakhirul, Encik Muhammad Faiz, and Encil Mohd Azrul from Science and Engineering Research Centre of USM for their invaluable assistance and cooperation provided in completing my final year project.

Last but not least, a special thanks to my family and friends for their unflinching support, endless motivation and continuous encouragement during my study. This accomplishment would not be possible without their understanding and assistance.

TABLE OF CONTENTS

Content	Page
DECLARATION	ii
ACKNOWLEDGEMENTS	iii
TABLE OF CONTENTS	iv
LIST OF TABLES	vii
LIST OF FIGURES	viii
LIST OF ABBREVIATIONS	xiii
LIST OF UNITS	xiv
ABSTRAK	xv
ABSTRACT	xvi
CHAPTER 1 INTRODUCTION	1
1.1 Background of Study.....	1
1.2 Problem Statement	3
1.3 Research Objectives	5
1.4 Thesis Outline	5
CHAPTER 2 LITERATURE REVIEW	6
2.1 Introduction	6
2.1.1 Manganese Doped Zinc Oxide	6
2.1.2 Hydrothermal Method	11
2.2 Physical Characterization of Manganese Doped Zinc Oxide Nanoparticles	17
2.2.1 Phase and Structural Analysis	17
2.2.2 Morphological and Elemental with Chemical Composition Analysis	21
2.2.3 Internal Structure Analysis.....	26
2.3 Supercapacitor.....	27

2.3.1	Hybrid Supercapacitors	33
2.3.2	Applications of Supercapacitors.....	34
2.4	Electrochemical Characterization of Manganese Doped Zinc Oxide Nanoparticles.....	35
2.4.1	Cyclic Voltammetry Analysis	36
2.4.2	Galvanostatic Charge-Discharge Analysis	39
CHAPTER 3	METHODOLOGY	43
3.1	Introduction	43
3.2	Materials and Equipment	43
3.3	Flowchart.....	46
3.4	Synthesis of Zn _{0.97} Mn _{0.03} O Nanoparticles by Hydrothermal Method.....	47
3.5	Preparation of Zn _{0.97} Mn _{0.03} O Nanoparticles Working Electrode	48
3.6	Physical Characterization of Zn _{0.97} Mn _{0.03} O Nanoparticles	49
3.6.1	Phase and Structural Analysis	49
3.6.2	Morphology and Elemental with Chemical Composition Analysis..	50
3.6.3	Internal Structure Analysis.....	51
3.7	Electrochemical Characterization of Zn _{0.97} Mn _{0.03} O Nanoparticles.....	51
3.7.1	Cyclic Voltammetry Analysis	53
3.7.2	Galvanostatic Charge-Discharge Analysis.....	53
CHAPTER 4	RESULTS AND DISCUSSIONS.....	54
4.1	Introduction	54
4.2	Physical Characterizations of Zn _{0.97} Mn _{0.03} O Nanoparticles	55
4.2.1	Visual Inspection.....	55
4.2.2	Structural Analysis	57
4.2.3	Morphological and Elemental with Chemical Composition Analysis.....	62
4.2.4	Particle Size Analysis.....	68
4.2.5	Internal Structure Analysis.....	70

4.3	Electrochemical Characterization of $Zn_{0.97}Mn_{0.03}O$ Nanoparticles.....	73
4.3.1	Cyclic Voltammetry Analysis	74
4.3.2	Galvanostatic Charge-Discharge Analysis	81
CHAPTER 5	CONCLUSION AND FUTURE RECOMMENDATIONS	85
5.1	Conclusion.....	85
5.2	Recommendations for Future Research	86
REFERENCES.....		87
APPENDICES.....		98

LIST OF TABLES

	Page
Table 2.1: Comparison of various electrochemical energy storage devices properties (González et al., 2016).....	29
Table 3.1: List of chemicals and raw materials used.	43
Table 3.2: List of equipment used.....	45
Table 4.1: (011) plane peak position, d-spacing and lattice parameters of Zn _{0.97} Mn _{0.03} O nanoparticles after different hydrothermal heat treatment temperature.	61

LIST OF FIGURES

	Page
Figure 2.1: Schematic representation of ZnO crystal structures: (a) Cubic rocksalt, (b) Cubic zinc blende and (c) Hexagonal wurtzite (d) Wurtzitic ZnO structure with lattice constants a in the basal plane and c in the basal direction (The yellow sphere and blue spheres represent zinc and oxygen atoms respectively) (Özgür et al., 2013).	10
Figure 2.2: Schematic diagram of (a) interstitial site and (b) substitutional site of Mn in the ZnO lattice after doping (Cheng et al., 2016).	10
Figure 2.3: Schematic representation of crystal growth mechanism under the hydrothermal environment (Li et al., 2015).	13
Figure 2.4: Schematic diagram of hydrothermal synthesis process of various nanostructures under different reaction parameters (Mohan et al., 2020).	15
Figure 2.5: Stepwise hydrothermal synthesis procedure (Rashid et al., 2021).	16
Figure 2.6: Schematic diagram of microwave-assisted hydrothermal method (Naresh et al., 2021).	17
Figure 2.7: XRD patterns of hydrothermal synthesized $Zn_{1-x}Mn_xO$ nanoparticles ($x= 0.01, 0.02, 0.03, 0.04$ and 0.05) (Senol et al., 2020).	20
Figure 2.8: 3D plot of XRD spectra for hydrothermal synthesized undoped ZnO nanoparticles and Mn-doped ZnO nanoparticles (2% 5% 15% Mn/ZnO ratio) (Abrinaei and Molahasani, 2018).	20
Figure 2.9: XRD pattern of undoped ZnO and Mn-doped ZnO with annealing temperature at 300, 500 and 600°C, (b) (100), (002) and (101) peak position shifting (Bordbar et al., 2015).	20
Figure 2.10: SEM images of ZnO nanoparticles with (a) 1 at%, (b) 2 at%, (c) 3 at%, (d) 4 at% and (e) 5 at% Mn doped (Senol et al., 2020).	22

Figure 2.11: FESEM image of (a) undoped ZnO nanoparticles and Mn-doped ZnO nanoparticles with (b) 2%, (c) 5% and (d) 15% of Mn/ZnO ratios (Abrinaei and Molahasani, 2018).	23
Figure 2.12: SEM micrographs of (a) ZnO, (b) $Zn_{0.75}Mn_{0.25}O_3$, (c) $Zn_{0.25}Mn_{0.75}O_3$, (d) MnO_2 , respectively (Rashid et al., 2021).....	23
Figure 2.13: SEM micrographs of $Zn_{0.50}Mn_{0.50}O_3$ at various magnifications (a)35000X, (b)5 000X, (c) 2500X, and (d) 120X (Rashid et al., 2021).	24
Figure 2.14: EDX spectra of the synthesized Mn-doped ZnO nanoparticles with different Mn doping concentrations (a) 1%, (b) 3% and (c) 5 at% (Senol et al., 2019).....	25
Figure 2.15: TEM image of (a) undoped, (b) 3 at% Mn-doped ZnO nanoparticles, HRTEM micrograph of (c) undoped, (d) 3 at% Mn-doped ZnO nanoparticles (Khan et al., 2018), and (e)TEM image of $Zn_{0.92}Mn_{0.08}O$ nanoparticles (Gao et al., 2016).....	27
Figure 2.16: Ragone plot of the power-energy density range for different electrochemical energy storage devices (Bokhari et al., 2020).	29
Figure 2.17: Classification of different types of supercapacitors and their representative electrode materials based on the charge storage mechanism that takes place in each class of supercapacitor (Bokhari et al., 2020).	30
Figure 2.18: Schematic illustration of (a) an electrostatic capacitor, (b) an electric double-layer capacitor, (c) a pseudocapacitor, and (d) a hybrid-capacitor (Zhong et al., 2015).....	31
Figure 2.19: (a) CV profiles for electrode material of $Zn_{1-x}Mn_xO_3$ nanoribbons with $x=0, 0.25, 0.50, 0.75$ and 1 at scan rate 5 mV/s, (b) CV profiles at different scan rate for $Zn_{0.5}Mn_{0.5}O_3$ nanoribbons sample (Rashid et al., 2021).	37
Figure 2.20: CV curve of ZnO/ MnO_x nanoflowers (a) at various scan rate and (b) in different potential window (Samuel et al., 2020).	38

Figure 2.21:	CV curves of (a) 3mM, (b)7mM (c) 5mM Mn-doped ZnO decorated CNFs at various scan rate in voltage range of 0–1.0 V (Samuel et al., 2019).	39
Figure 2.22:	(a) GCD profiles of $Zn_{0.50}Mn_{0.50}O_3$ s at current density of 2, 3.3 and $5.3Ag^{-1}$ and, (b) Calculated specific capacitance as a function of current density for $Zn_{1-x}Mn_xO_3$ (Rashid et al., 2021).	40
Figure 2.23:	(a) Comparison of GCD curves of ZnO NFs at $1 Ag^{-1}$, (b) ZnO/MnO _x NFs at $3 Ag^{-1}$ in 0.5, 0.7 and 0.9 potential windows at current density of $3 A g^{-1}$, (c)Potential window-dependence of ZnO NFs and, (d) ZnO/MnO _x NFs capacitance at different current densities (Samuel et al., 2020).	41
Figure 2.24:	(a) GCD profiles of 5mM Mn-doped ZnO@CNF at different current densities and (b) The specific capacitances of Mn-doped ZnO@CNF versus current density (Samuel et al., 2019).	42
Figure 3.1:	Overall flowchart of experimental work.	46
Figure 3.2:	Schematic diagram on all procedures in the synthesis of $Zn_{0.97}Mn_{0.03}O$ nanoparticles by hydrothermal method.	48
Figure 3.3:	Schematic diagram of electrochemical characterization set-up of $Zn_{0.97}Mn_{0.03}O$ nanoparticles.	52
Figure 3.4:	Experimental three electrodes system of $Zn_{0.97}Mn_{0.03}O$ -Graphene-PVDF // 1M KOH // Hg/HgO/Pt cell set-up for electrochemical characterization.	52
Figure 4.1:	Optical images of $Zn_{0.97}Mn_{0.03}O$ nanoparticles synthesized at different hydrothermal heat treatment temperature of (a) 80, (b) 100, (c) 120, (d) 140, (e) 160, (f) 180, and (g) 200 °C.	56
Figure 4.2:	XRD patterns of (a) $Zn_{0.97}Mn_{0.03}O$ nanoparticles after different hydrothermal heat treatment temperatures	58
Figure 4.3:	XRD diffraction peak at (011) plane.	59
Figure 4.4:	Intensity in counts per second for diffraction peaks at (011) plane... ..	60

Figure 4.5:	FESEM image of $Zn_{0.97}Mn_{0.03}O$ nanoparticles after different hydrothermal heat treatment temperatures ($T = 80, 100, 120, 140, 160, 180$ and $200\text{ }^{\circ}C$) with 40000X magnification.....	64
Figure 4.6:	EDX spectrum of $Zn_{0.97}Mn_{0.03}O$ nanoparticles after different hydrothermal heat treatment temperatures of (a) 80, (b) 100, (c) 120, (d) 140, (e) 160, (g) 180, and (g) 200 $^{\circ}C$	67
Figure 4.7:	Particle size distribution of $Zn_{0.97}Mn_{0.03}O$ nanoparticles after different hydrothermal heat treatment temperatures.....	68
Figure 4.8:	Variation in average particle size of $Zn_{0.97}Mn_{0.03}O$ nanoparticles after different hydrothermal heat treatment temperatures.	69
Figure 4.9:	HRTEM images of $Zn_{0.97}Mn_{0.03}O$ nanoparticles after 160 $^{\circ}C$ of hydrothermal heat treatment at magnifications (a) 15000 X (b) 43000 X, (c) 97000 X, (d) 195000 X, (e) 490000 X, (f) 690000 X, (g) 1050000 X and (h) representative hexagonal structure nanoparticle in red-dotted circle.	73
Figure 4.10:	CV profiles for cell of $Zn_{0.97}Mn_{0.03}O$ (hydrothermal heat treated at 160 $^{\circ}C$)-Graphene-PVDF // 1M KOH // Hg/HgO/Pt at different scan rates (10, 20, 40, 60, 80, and 100 $mV\ s^{-1}$).....	75
Figure 4.11:	CV profile of for cell of $Zn_{0.97}Mn_{0.03}O$ (hydrothermal heat treated at 160 $^{\circ}C$)-Graphene-PVDF // 1M KOH // Hg/HgO/Pt at scan rate of 10 $mV\ s^{-1}$	76
Figure 4.12:	CV profile for cells of $Zn_{0.97}Mn_{0.03}O$ (hydrothermal heat treated at 160 $^{\circ}C$)-Graphene-PVDF // 1 M KOH // Hg/HgO/Pt and Ni // 1 M KOH// Hg/HgO/Pt at scan rate of 10 $mV\ s^{-1}$	76
Figure 4.13:	CV profile for cell of $Zn_{0.97}Mn_{0.03}O$ (hydrothermal heat treated at 160 $^{\circ}C$)-Graphene-PVDF // 1 M KOH // Hg/HgO/Pt at scan rate of 10 $mV\ s^{-1}$ and 100 $mV\ s^{-1}$	78
Figure 4.14:	Variation in specific capacitance of $Zn_{0.97}Mn_{0.03}O$ nanoparticles determined from the CV voltammogram at different scanning rates of 10, 20, 40, 60, 80, and 100 $mV\ s^{-1}$	80

Figure 4.15:	GCD profiles for cell of $Zn_{0.97}Mn_{0.03}O$ (hydrothermal heat treated at $160^{\circ}C$)-Graphene-PVDF // 1 M KOH // Hg/HgO/Pt at different current densities of 0.4, 0.8, 1.2, 1.6, 2.0 and $2.4 A g^{-1}$	83
Figure 4.16:	Discharging curves for cell of $Zn_{0.97}Mn_{0.03}O$ (hydrothermal heat treated at $160^{\circ}C$)-Graphene-PVDF // 1 M KOH // Hg/HgO/Pt at different current densities of 0.4, 0.8, 1.2, 1.6, 2.0 and $2.4 A g^{-1}$	84
Figure 4.17:	Variation in specific capacitances of $Zn_{0.97}Mn_{0.03}O$ nanoparticles obtained from GCD profiles at different current densities of 0.4, 0.8, 1.2, 1.6, 2.0 and $2.4 A g^{-1}$	84

LIST OF ABBREVIATIONS

AC	Activated Carbon
CE	Counter Electrode
CNF	Carbon Nanofiber
CNT	Carbon Nanotube
CP	Conducting Polymer
CV	Cyclic Voltammetry
ELDC	Electrochemical Double-Layer Capacitor
EDX	Energy-Dispersive X-Ray Spectroscopy
FESEM	Field Emission Scanning Electron Microscope
GCD	Galvanostatic Charge-Discharge
GO	Graphene Oxide
HRTEM	High-Resolution Transmission Electron Microscope
ICSD	Inorganic Crystal Structure Database
JCPDS	Joint Committee on Powder Diffraction Standards
NP	Nanoparticle
NF	Nanoflower
RE	Reference Electrode
SEM	Scanning Electron Microscopy
TEM	Transmission Electron Microscope
TM	Transition Metal
WE	Working Electrode
XRD	X-ray Diffraction

LIST OF UNITS

A	Ampere
A g ⁻¹	Ampere per gram
°	Degree
°C	Degree Celsius
F g ⁻¹	Farad per gram
g	Gram
mV s ⁻¹	Millivolt per second
nm	Nanometer
Ω	Ohm
%	Percentage
pH	Potential of hydrogen
rpm	Revolution per minute
V	Voltage
Wh kg ⁻¹	Watt-hour per kilogram
W kg ⁻¹	Watt per kilogram

NANOPARTIKEL ZINC OXIDE TERSINTESIS DARIPADA HIDROTERMA DENGAN DOPING MANGAN UNTUK SUPERKAPASITOR

ABSTRAK

Logam peralihan oksida telah menjadi tarikan sebagai superkapasitor elektrod terutamanya zink oksida (ZnO) disebabkan aktiviti elektrokimia yang baik, mesra alam sekitar dan murah, ZnO tulen yang mempunyai kekonduksian elektrik yang lemah dan kadar cas-pelepasan kapabiliti yang rendah masih cabaran dalam aplikasi elektrokimia. Di sini, kaedah hidrotermal telah digunakan untuk menghasilkan zink oksida mangan (Mn) nanopartikel pada kepekatan doping 3 peratusan atom ($Zn_{1-x}Mn_xO$, $x=0.03$). Kesan suhu rawatan hidrotermal (80, 100, 120, 140, 160, 180 hingga 200 °C) ke atas sifat fizikal dan elektrokimia nanopartikel $Zn_{0.97}Mn_{0.03}O$ telah disiasat. Analisis struktur menunjukkan kejayaan penggabungan ion Mn ke dalam struktur wurtzite heksagon ZnO dengan kandungan campuran yang rendah. Unsur konstituen utama dalam nanopartikel disintesis telah disahkan sebagai Mn, Zn dan O oleh pencirian unsur. Analisis morfologi menunjukkan pembentukan sfera atau heksagon partikel dengan saiz seragam dalam $Zn_{0.97}Mn_{0.03}O$ yang disintesis pada 160 °C. Kajian elektrokimia menunjukkan bahawa $Zn_{0.97}Mn_{0.03}O$ nanopartikel selepas rawatan hidrotermal 160 °C mempunyai tindak balas yang sangat baik terhadap sifat pseudocapacitif. Analisis voltametri siklik menunjukkan bahawa nanopartikel mempamerkan peningkatan prestasi yang ketara sebagai superkapasitor elektrod dengan kapasitansi spesifik yang cemerlang iaitu 974.2 F g^{-1} yang diukur pada kadar imbansan 10 mV s^{-1} kerana Mn ion mengurangkan rintangan pemindahan cas. $Zn_{0.97}Mn_{0.03}O$ elektrod menunjukkan reaksi redoks yang baik dalam pelepasan cas galvanic analisis. Ciri-ciri yang impresif menunjukkan $Zn_{0.97}Mn_{0.03}O$ nanopartikel adalah calon yang menjanjikan untuk aplikasi superkapasitor.

HYDROTHERMAL SYNTHESIZED ZINC OXIDE NANOPARTICLES WITH MANGANESE DOPING FOR SUPERCAPACITOR

ABSTRACT

Transition metal oxides have drawn appealing attraction as supercapacitor electrode especially zinc oxide (ZnO) due to their good electrochemical activity, environmentally friendly and cheap, but the weak conductivity and low charge-discharge rate capability of pure ZnO remain challenging in electrochemical applications. Herein, facile hydrothermal method was applied to synthesized manganese (Mn) doped ZnO nanoparticles at doping concentration of 3 at% ($Zn_{1-x}Mn_xO$, $x=0.03$). The effect of hydrothermal heat treatment temperature (80, 100, 120, 140, 160, 180 to 200 °C) on physical and electrochemical properties of $Zn_{0.97}Mn_{0.03}O$ nanoparticles was investigated. The structural analysis revealed the success of Mn ions incorporation into ZnO hexagonal wurtzite structure with low impurities content. Major constituent elements in the synthesized nanoparticles were confirmed as Mn, Zn and O by elemental composition characterization. The morphological analysis demonstrated the formation of spherical or hexagonal particles with uniform size in the $Zn_{0.97}Mn_{0.03}O$ synthesized at 160 °C. Electrochemical studies showed that hydrothermal heat treated $Zn_{0.97}Mn_{0.03}O$ nanoparticles at 160 °C have excellent response towards pseudocapacitive nature. Cyclic voltammetry analysis showed that the nanoparticles exhibited significantly improved performance as supercapacitors electrode with excellent specific capacitance of 974.2 F g^{-1} measured at scan rate of 10 mV s^{-1} due to the Mn ions help in decreasing the charge transfer resistance. The $Zn_{0.97}Mn_{0.03}O$ electrode shows good redox behaviour in galvanostatic charge-discharge analysis. Such impressive properties lead $Zn_{0.97}Mn_{0.03}O$ nanoparticles to be considered as a promising candidate for supercapacitor applications.

CHAPTER 1

INTRODUCTION

1.1 Background of Study

The digital transformation in the epoch of humankind caused the growing demand for electrical energy. Supercapacitors are recognized as one of the major classes of electrochemical energy storage devices popular for delivering high energy and power density on demand at lower cost. They are safer, possess higher power density with rapid charge/discharge capability and excellent stability compared to conventional capacitor and batteries such as dielectric capacitor, secondary cell, fuel cells and lithium-ion batteries but poorer on energy density (Angelin et al., 2020). These unique properties leading supercapacitor a potential application in various areas include portable electronic devices, low-emission electric/hybrid vehicles, backup power supplies, regenerative braking systems, renewable energy systems (Anandhi et al., 2019).

It is worth noting that the selection of electrode materials in supercapacitors plays a vital role towards their capacitive performance. The electrode materials should offer fascinating characteristic such as high electrical conductivity, high specific surface area, suitable chemical stability in order to fabricate highly performing supercapacitor. Cost effective and eco-friendly are another criteria to be consider (Forouzandeh et al., 2020). Transition metal oxides are excellent option for electrode fabrication in high energy and power supercapacitors. Examples transition metal oxide commonly explored as electrode materials are ruthenium oxide (RuO_2) (Patake et al., 2009), manganese oxide (MnO_2) (Jiang and Kucernak, 2002, Yan et al., 2010), nickel oxide (NiO) (Nelson and Owen, 2003, Patil et al., 2008), and ZnO (Subagio et al., 2018).

Zinc Oxide (ZnO) appears to be a promising electrode material because of their diverse properties. ZnO is an intrinsic n-type semiconductor with wide bandgap (3.7 eV),

large exciton binding energy (60 meV), high electrochemical stability and excellent optical absorption in the UV range and transparency (Zhai et al., 2020). ZnO are being utilize in many applications like solar cells, photocatalyst, antibacterial activity, gas sensors (Angelin et al., 2020, Mote et al., 2016). The characteristic of low cost, abundance in nature, non-toxicity, environmental friendliness and high theoretical capacitance performance also make it suitable for supercapacitor electrode material (Shunmuga Sundaram et al., 2019, Wang et al., 2011). However, pure ZnO have poor electrical conductivity, severe pulverization during charging/discharging causing difficulty in supercapacitor application (Ghorbani et al., 2017). Hence, ZnO is suggested to introduce with dopants like metals or transition metal into the structure of ZnO to solves these problems.

A variety of metal element such as iron, manganese (Mn), cobalt, zirconia, cadmium, silver, titanium can be added into ZnO nanostructure by doping to enhance the efficiency and electronic, magnetic and optical properties of the material (Angelin et al., 2020). Mn has been found to be used in ZnO in the last two decades. The structural, optical, morphological and supercapacitor properties of ZnO can be modified by inclusion of Mn dopants to enhance its supercapacitor applications. Owing to the high magnetic moment of Mn ions, the inclusion of Mn ions into the Zn host structure will not affect the original Zn structure. According to Mote et al. (2016), electrical properties of ZnO can be altered by varying the concentration of Mn dopant. An optimal Mn doping concentration into ZnO nanoparticles is employed in this work which is 3 at% as this value is the solubility limit of transition metal ion in ZnO (Rajalakshmi and Angappane, 2013). According to Yuwita et al. (2020) and Xin et al. (2014), ZnO doped with transition metal ions of Mn is fabricated using doping concentration of 3 at% since the secondary phase has been observed in the XRD pattern of ZnO with higher Mn ion percentage. This

indicates that Mn exceeding the maximum solubility are unable to incorporate in the ZnO matrix.

The shape, size, dimensionality and structure of the powder should be precisely regulated by fabrication methods to produce Mn-doped ZnO nanoparticles with ideal properties. Fabrication techniques such as sol-gel (Abdel-Galil et al., 2015), thermal evaporation (Shen et al., 2005), co-precipitation (Djaja et al., 2013), spray pyrolysis (Kodas, 1989), solid-state sintering method (Chattopadhyay et al., 2009) and hydrothermal method (Alver et al., 2016) have been utilized to synthesize ZnO nanoparticles. Each approach has their own different advantages and drawbacks that must be addressed such as electrochemical properties, crystallinity and morphology of nanomaterials.

Hydrothermal synthesis is a simple and powerful technique that gained popularity recently in the fabrication nanomaterials. This technique depends on chemical reactions and solubility changes of compounds in a sealed aqueous solution above ambient temperature and pressure. The liquid phase chemical processes in the hydrothermal synthesis method enable precisely regulation of the nanomaterials compositions to be produced (Ng et al., 2020). The advantages of hydrothermal method over conventional synthesis method are uniform morphology, low cost, high productivity and easy to control size (Yang et al., 2016). In this study, hydrothermal synthesis route is being choose for preparation ZnO nanoparticles.

1.2 Problem Statement

Zinc oxide (ZnO) as a transition metal oxide is a rising star of supercapacitor electrode material owing to its outstanding properties and versatility. However, there are some challenges in developing ZnO for supercapacitor application because of the pure

ZnO exhibit weak conductivity, poor reaction kinetics and low charge-discharge rate capability performance resulting in relatively low energy density (Wei et al., 2021). Incorporation of manganese (Mn) ions into ZnO lattice is a potential solution for improving electrochemical properties of ZnO. The optimum doping concentration of Mn into ZnO lattice used in this work is 3 at% synthesizing Mn-doped ZnO nanoparticles, $\text{Zn}_{0.97}\text{Mn}_{0.03}\text{O}$. This is value represents the solubility limit of transition metal ion in ZnO. Impurities phases can be observed when degree of doping exceeds this level (Rajalakshmi and Angappane, 2013, Yuwita et al., 2020).

Various routes have been employed for synthesis of Mn-doped ZnO nanoparticles in previous studies especially sol-gel method. However, this method involves many preparation steps, relatively long process duration, and expensive and not suitable for bulk production. Hydrothermal method is a promising route for synthesizing nanostructures. There are notable advantages of hydrothermal method over other conventional method including simple mode of operation, easy modification of nanoparticles size and shape, time and energy saving for nanoparticles fabrication in large scale. Synthesizing parameters such as pH value, heat treatment duration, temperature plays a significant role in the formation of nanoparticles and varies their physical properties. There are limited studies done on the effect of hydrothermal heat treatment temperature on physical properties of $\text{Zn}_{0.97}\text{Mn}_{0.03}\text{O}$ nanoparticles.

To date, the electrochemical properties of $\text{Zn}_{0.97}\text{Mn}_{0.03}\text{O}$ nanoparticles as supercapacitor have not been a research focus. The structure, morphology, crystallinity, particles size and other physical properties of $\text{Zn}_{0.97}\text{Mn}_{0.03}\text{O}$ nanoparticles greatly influenced their electrochemical properties. In this work, hydrothermal method is used with different heat treatment temperature to identify the ideal synthesizing temperature for $\text{Zn}_{0.97}\text{Mn}_{0.03}\text{O}$ nanoparticles and the electrochemical properties are investigated.

1.3 Research Objectives

The objectives of this study are:

- i. To synthesize Mn-doped ZnO nanoparticles, $\text{Zn}_{0.97}\text{Mn}_{0.03}\text{O}$ with hydrothermal method at different heat treatment temperatures.
- ii. To perform characterization on the phase, structure and morphology of $\text{Zn}_{0.97}\text{Mn}_{0.03}\text{O}$ nanoparticles.
- iii. To investigate the electrochemical properties and cycle life performance of $\text{Zn}_{0.97}\text{Mn}_{0.03}\text{O}$ as supercapacitor.

1.4 Thesis Outline

This research involves the synthesis of Mn-doped ZnO nanoparticles at doping concentration $x = 0.03\%$ through hydrothermal technique for supercapacitor application. In this research work, there are five chapters that fully describe each key aspect of the research.

The first chapter (Chapter 1) begins with an introduction of supercapacitors and ZnO nanoparticles. In Chapter 2, a comprehensive literature review on manganese doped zinc oxide nanoparticles, hydrothermal method, supercapacitors and characterization techniques are presented. Next, Chapter 3 covers the detailed experimental procedure, characterization approaches applied in this research. The chemicals, materials and equipment used in the study are also present in this chapter.

In Chapter 4, the results and findings of phase, morphological, structural characterization, electrochemical characterization are analyzed and discussed. Finally, the results of the research work and recommendations for future improvement are summarized in the last chapter (Chapter 5).

CHAPTER 2

LITERATURE REVIEW

2.1 Introduction

Key aspects of manganese (Mn) doped zinc oxide (ZnO) nanoparticles and supercapacitor are covered in this chapter. An overview of current knowledge associated with Mn-doped ZnO nanoparticles, hydrothermal method and supercapacitors is presented aiming to assist the discussions in following chapters. There are several characterization techniques are used in this study, including phase and structural analysis, morphological and elemental with chemical composition analysis, internal structure and crystalline phase analysis, and electrochemical characterization for supercapacitors.

2.1.1 Manganese Doped Zinc Oxide

ZnO is a famous metal-oxide-based semiconductor from group II-IV that exhibits variety potential applications in different areas, hence has inspired interest in studying its supercapacitor performance thanks to its remarkable physical and electrochemical properties. Cubic rocksalt, cubic zinc blende, and hexagonal wurtzite are three distinct crystal structure of ZnO as shown in Figure 2.1.

Hexagonal wurtzite form of ZnO is the most thermodynamically stable phase under ambient conditions. This wurtzite structure made up two interpenetrating hexagonal closed packed sublattices (hcp) every zinc atom where each sublattice composed of one type of atom (Zn or oxygen, O) offset from each other along the threefold c-axis. It also can be described as a series of alternating staking planes consist of tetrahedral coordinated zinc cation and oxygen cation, in which zinc atom is surrounded by four oxygen atoms at the corners of tetrahedron and vice versa. The tetrahedral coordination with sp^3 covalent bending results in a polar symmetry along the

hexagonal axis. This polarity is crucial for various properties of ZnO, which responsible for piezoelectricity, spontaneous polarization, plasticity, crystal growth, etching and defect generation. ZnO present in Rocksalt or Rochelle salt (NaCl) structure at high pressure condition. On the other hand, zinc blende ZnO structure is a metastable phase which only can be stabilized through heteroepitaxial growth on cubic substrate like ZnS, GaAs/ZnS and Pt/Ti/SiO₂/Si (Morkoç and Özgür, 2009).

ZnO are being utilize in many applications like solar cells, photocatalyst, antibacterial activity, gas sensors, light-emitting devices, conductive thin films, blue or ultraviolet laser material, piezoelectric devices and field effective transistor (Mote et al., 2016, Angelin et al., 2020). ZnO can appears in a variety of nanostructures like wires (Li et al., 2017), tubes (Yu et al., 2005), rods (Gonzalez-Valls et al., 2011), belts (Kong et al., 2004), rings, springs (Kong and Wang, 2003), flowers (Samuel et al., 2020), and peanuts (Prabhu et al., 2015) forms. ZnO with particle size in nanoscale range have been a research focus due to their special characteristic. Such as high exciton binding energy of 60 meV, wide direct band gap of 3.37eV, low growth temperature, non-toxicity, low cost as compared to other metal oxides, high abundance, large electron mobility, polar nature, good chemical stability and eco-friendliness (Ni et al., 2005, Xin et al., 2014). Besides, the high theoretical capacitance performance, good electrochemical stability and high specific energy density make ZnO nanoparticles to a promising electrode material for supercapacitor application (Li et al., 2013, Li et al., 2020).

Although the further development of ZnO electrodes has some progress, pure ZnO still suffered weak conductivity, poor cycling stability and low reversible capacity at high current density, serious pulverization in charge-discharge process resulting in low energy density (Wei et al., 2021). The existence of intrinsic defects in ZnO such as oxygen

vacancies, zinc vacancies and zinc interstitials may cause the pure ZnO unable to fulfil the ideal standard for industrial application (Abinaya et al., 2017).

Several strategies have been proposed to tackle these issues and enhance the functionality of semiconductors. Among the strategies, incorporation of suitable non-metallic or metallic dopants into the host material is a widely used method to improve the properties of ZnO greatly and alter ZnO to become suitable materials in different applications particularly in energy field. Doping is a process of intentionally introducing a small concentration of impurities into the host material for the modification of nanoparticles properties. Generally, doping level has an upper bound, which refers to the maximum amount of the dopant in the host material with formation of one phase only, also known as solubility limit (Su, 2019, Mouritz, 2012). Transition metals such as Fe, Mn, Co, Cr, Cd, Ag, Ga, In, Ti, Ni and Sn have been introduced into wide band gap semiconductors by doping (Mote et al., 2016, Irshad et al., 2018). Ni has been successfully combined ZnO, achieving better water splitting activity and supercapacitor properties (Neelakanta Reddy et al., 2018). ZnO doped with Zr electrode demonstrate outstanding specific capacitance, current density and electrochemical reversible nature (Angelin et al., 2020). Mohammadigharehbagh et al. (2021) have synthesized Fe-doped ZnO magnetic nano-crystal thin films and reported they possess ferromagnetism characteristics at room temperature with great magnetic moment and electrical conductivity.

Researches are putting effort to develop more reliable ZnO for supercapacitor applications by doping it with transition metal ions. Among the transition metals, Mn acts as a promising dopant for ZnO nanostructures. Mn ions is an important dopant for adjusting the structural and optical properties of ZnO nanostructure (Toufiq et al., 2021). A key consideration for choosing of manganese as dopant into ZnO host lattice is the

ionic radius of Mn^{2+} ion (0.066 nm) is close to the ionic radius of Zn^{2+} ion (0.060 nm) (Aksoy and Caglar, 2019). Mn^{2+} ion have similar oxidation state as the Zn^{2+} ion, the Mn^{2+} ion can fully compensate the charge when it substitutionally replaced the Zn^{2+} (Shunmuga Sundaram et al., 2019). Mn exhibits the highest number of oxidation state of +2 to +7, among the 3d-series elements making it a wise option to improve the ZnO redox nature (Mary and Bose, 2017).

Doping of Mn ions will improve the electrical properties by forming additional intrinsic defects or accumulate impurities into lattice site. The band gap of the ZnO host metal oxide also can be shift to visible light region and promote the interfacial charge-transfer mechanism. Introduction of Mn ions into ZnO will change the host material band gap such that 3.37eV to 3.70eV. Furthermore, addition of Mn also influences the emission characteristics by offering an effective pathway for electron-hole recombination through the dopant Mn d-levels (Ali et al., 2012). Mn with partially filled valence 3d-orbitals have unpaired electrons. When Mn^{2+} substitute the lattice site of Zn^{2+} , the strong 3d-orbitals of Mn^{2+} and the p-orbitals of the adjacent anion can influence the internal electronic structure of the ZnO host material. The optical and electronic properties of semiconductors can be further modified by altering the particle size in the nanometer range. The quantum confinement of electronic states on various Mn-doped semiconductor nanoparticles has also been proven in studies that can modify the properties of these samples, such as the band gap (Shunmuga Sundaram et al., 2019). Figure 2.2 shows the interstitial and substitutional site of Mn in the ZnO lattice after doping.

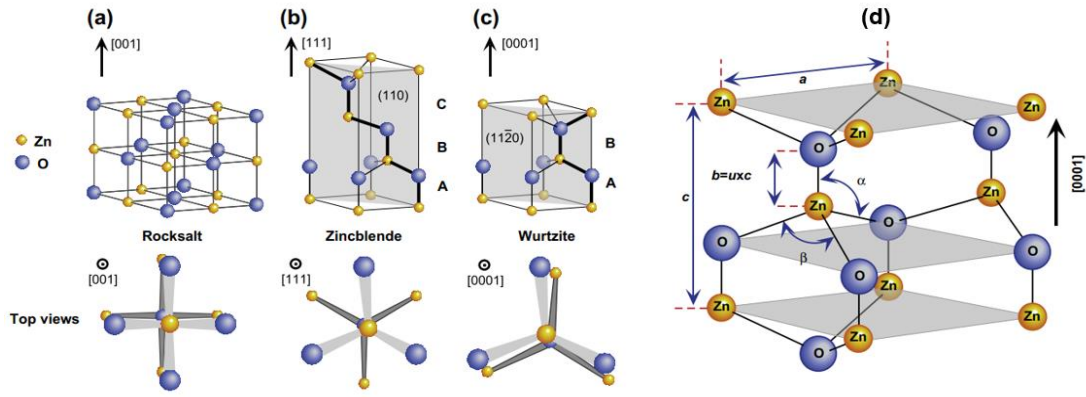


Figure 2.1: Schematic representation of ZnO crystal structures: (a) Cubic rocksalt, (b) Cubic zinc blende and (c) Hexagonal wurtzite (d) Wurtzitic ZnO structure with lattice constants a in the basal plane and c in the basal direction (The yellow sphere and blue spheres represent zinc and oxygen atoms respectively) (Özgür et al., 2013).

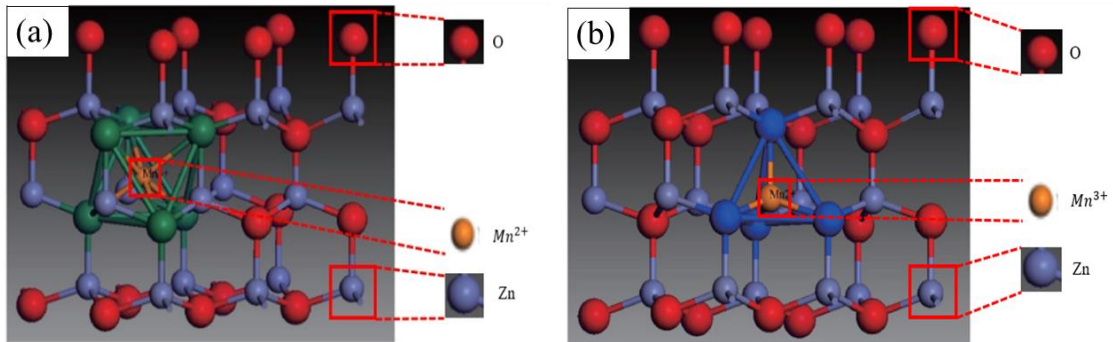


Figure 2.2: Schematic diagram of (a) interstitial site and (b) substitutional site of Mn in the ZnO lattice after doping (Cheng et al., 2016).

Yuwita et al. (2020) have reported the solubility limit of Mn into ZnO is 0.03 molar ratio since impurity corresponding to the ZnMnO_3 is present in the XRD pattern when Mn doping concentration is at 3 at%. In a study of transition metal ion doping in ZnO, the doping concentration applied is 3 at% due to secondary phase formation in the over-doped (>3 at%) ZnO matrix (Rajalakshmi and Angappane, 2013). Xin et al. (2014) compared the effect of Mn doping in ZnO at different concentration and successfully reveal that 3 at% Mn doping have the most significant enhancement in crystallinity quality. Thus, ZnO matrix is doped with Mn at 3 at% in this paper.

2.1.2 Hydrothermal Method

Selection of appropriate synthesis method is important in order to obtain to high stable, shape-controlled and monodisperse Mn-doped ZnO nanoparticles. Basically, there are two types of synthesise method for metal oxide nanoparticles, physical route and chemical routes (Parashar et al., 2020). Physical routes are mainly based on top-down approach which involves breaking down of bulk counterpart of any material into fine nanoparticles. Examples of physical routes synthesis methods are electron beam evaporation, ball milling, sputtering, laser ablation and electrospraying. On the contrary, chemical routes relies on a bottom-up approach which refers to a distribution of varying size nanoparticles are generated from the assembling of the small components of atoms-by-atom or molecules-by-molecules. Chemical routes also involve chemical reaction among atom, ions or molecules of the starting salt to synthesize the nanoparticles (Pal Singh et al., 2020). Sol-gel method, hydrothermal method, co-precipitation method, microemulsion method and chemical vapor deposition are classified under chemical routes.

In recent years, great number of literatures have been employed sol-gel, co-precipitation, thermal decomposition and etc to prepared ZnO nanoparticles. Ali et al. (2012) have fabricated Mn-doped ZnO nanoparticles in an ethanolic solution through a sol-gel method using zinc acetate and manganese acetate as precursor. Pure and Mn-doped ZnO nanoparticles (1 and 2 at%) were successfully synthesized by using sol-gel technique and zinc acetate dihydrate and manganese acetate tetrahydrate as starting material, reported synthesized powder having an average size of 74 – 93 nm. Pure ZnO nanoparticles with particles size of 35nm have been fabricated via a coprecipitation method where zinc (II) nitrate hexahydrate, sodium hydroxide (NaOH) and polyethylene glycol (PEG) used as precursors and distilled water acts as solvent (Devi and Velu, 2016).

Thermal decomposition method to produce undoped ZnO nanoparticles with oleic acid, oleylamine, 1,2-dicane diol, zinc acetylacetonate as precursor and octadecylene, benzyl ether as solvent (Zong et al., 2019). Aghababazadeh et al. (2006) fabricated ZnO nanoparticles by using mechanochemical method which involves milling of starting material milled the starting powder such as anhydrous ZnCl_2 , Na_2CO_3 , NaCl as diluent and subsequently precursors are heat treated.

However, there are few literature reports on the detailed procedures for preparing ZnO nanoparticles using hydrothermal method. Therefore, this research uses the hydrothermal process to fabricate Mn-doped ZnO nanoparticles. Among the fabrication techniques, hydrothermal synthesis is a frequently employed method for preparing powdery nanostructures (Ng et al., 2020). Generally, hydrothermal process involves chemical reaction in solvents contained in a sealed vessel in which the temperature of solvent is raised beyond the boiling point through heating concurrently with elevated pressure (Ijaz, Khalid & Chaudhry, 2019). The sealed reaction vessel used in hydrothermal synthesis usually known as an autoclave or high-pressure bomb, it offers a closed system and high pressure to encourage chemical reactions between the liquid precursors (Yang et al., 2016). Generally, the sealed reaction vessel are metallic autoclaves lined with Teflon or alloy, or together with Teflon, platinum, gold, or silver can, beaker or tube which help in prevent damage of the autoclave body by corrosive solvent kept in critical temperature and pressure.

Basically, the fine crystals formation by hydrothermal technique is a crystallization process which comprises of two steps as depict in Figure 2.3: crystal nucleation and consequent crystal growth. Hydrothermal synthesis begins with mixing of precursors and appropriate agents in a solvent to obtain a proper ratio crystalline nanostructure. Then, the mixture is placed into an autoclave and heated in an oven at a

predetermined temperature, autogenous pressure and duration. The reactants are first dissolved in the aqueous media by higher temperature, forming ions or molecules. Consequently, temperature gradient between the top and low region of the reaction vessel separates and moves ions and molecules to low temperature area (upper region) by convection at which seed crystals growth occurs and forms supersaturated solution. At the growth interface, ions or molecules are adsorbed, degraded and desorbed. Finally, crystallization happens of dissolved substance happened at lower temperature.

The formation of nanomaterials in hydrothermal method can occur over a broad range of temperature, from room temperature to extremely high temperature (Gan et al., 2020). The metal salts can be hydrolysed and dehydrated by water at elevated temperatures and pressures. The high temperatures in hydrothermal environment can accelerate dehydration and causes the reactants to have enhanced diffusivity or reactivity (Movlaee et al., 2017). Eventually, supersaturation is created by the low solubility metal oxides obtained in the aqueous solvent. Nucleation takes place under when solution becomes supersaturated. Then, the solute precipitates grow sequentially or simultaneously into crystal cluster and macroscopic size through a series of events involving the integration of growth units as illustrated in Figure 2.3 (Li et al., 2015).

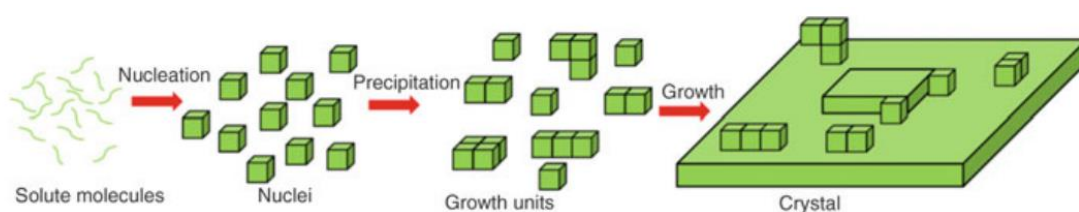


Figure 2.3: Schematic representation of crystal growth mechanism under the hydrothermal environment (Li et al., 2015).

This technique has been extensively used for direct generation of submicron or nanosized metal oxide particles which does not require post-heat treatment step. It can be used to synthesize nanomaterials that are unstable at high temperatures. Hydrothermal

technique allows well controlled of nanomaterial chemical composition via the liquid phase or multiphase chemical reactions. The morphology, grain size, surface chemistry, crystalline phase can be easily altered in hydrothermal synthesis by controlling of reaction parameters like temperature, time, pressure, solvent, surfactant, solution composition and aging time (Boudiba et al., 2012). High vapor pressure nanomaterials also can be generated with minimal material loss (Gan et al., 2020). The benefits of hydrothermal method also include low cost, environmental benignity, high yield, excellent product dispersion, simplicity of process and equipment, versatility (Yang et al., 2016, Ijaz et al., 2020, Kaur et al., 2020).

To date, several researchers have chosen hydrothermal process to create ZnO nanoparticles since it is a relatively simple and cost-effective process for bulk production. Different precursors solutions are used including acetate, chloride and nitrate to prepare Mn-doped ZnO nanoparticles with different electrochemical performance and morphology. A conventional hydrothermal synthesis process is illustrated in Figure 2.4.

The effect of doping concentration on structural, optical and photocatalytic properties of Mn-doped ZnO nanoparticles synthesized by hydrothermal technique at 100 °C for 12 hours and following calcination at 500 °C have been studied by Senol et al. (2020). High-quality wurtzite structure was observed from the doped ZnO nanoparticles which showed the successful doping process. It is reported that the maximum band gap occurred at 3% Mn doping, while maximum particle size and highest value of Urbach energy was obtained at 5% Mn doping.

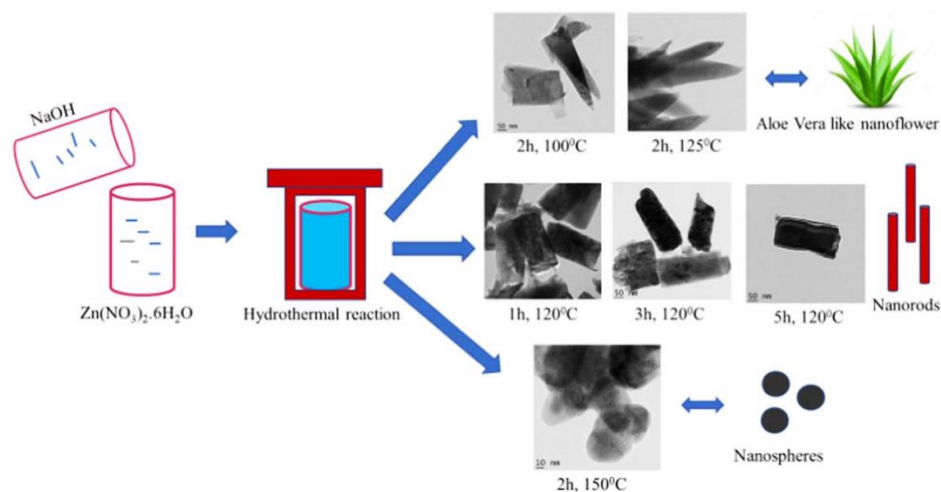


Figure 2.4: Schematic diagram of hydrothermal synthesis process of various nanostructures under different reaction parameters (Mohan et al., 2020).

Another successful hydrothermal synthesis of Mn-doped ZnO nanoparticles was demonstrated by Abrinaei and Molahasani (2018). They produced 2, 5, and 15% Mn/ZnO ratios nanoparticles in the presence of alkaline with mixing zinc chloride hexahydrate, manganese dichloride tetrahydrate and potassium hydroxide (KOH) in distilled water to study their structural, linear, and non-linear optical properties. Then, cetyltrimethylammonium bromide (CTAB) was added in stirring condition at room temperature into the solution. During the reaction, the pH value is maintained at 8-9. Hydrothermal treatment was done for the mixture contained in 150 mL Teflon-lined stainless-steel autoclave at 120 °C for 5 h. Next, the autoclave was naturally cooled down. The precipitates were collected and repeated washed with ethanol and distilled water. The as-formed precipitates were dried at 50 °C for 5 h in an oven to produce powder form Mn-doped ZnO nanoparticles. This method led to homogeneously distributed spherical nanoparticles with average diameters of 20–38 nm.

Recently, Rashid et al. (2021) reported on the inductive effect in Mn-doped ZnO nanoribbon arrays grown on nickel foam by a cost effective stepwise hydrothermal procedure outlined in Figure 2.5, for enhanced capacitive and high specific energy

supercapacitor. The nickel foam substrate was first pre-treated with hydrochloric acid (HCl) solution and Mn-doped ZnO nanoribbon arrays is prepared on nickel foam through hydrothermal reaction of zinc nitrate hexahydrate, manganese sulphate monohydrate, KOH and urea at 200 °C for 24 h and following annealing treatment at 450 °C for 5 h. The electrochemical studies indicates that the insertion of dopants in ZnO significantly boost the electrical conductivity and capacitive performance of electrode.

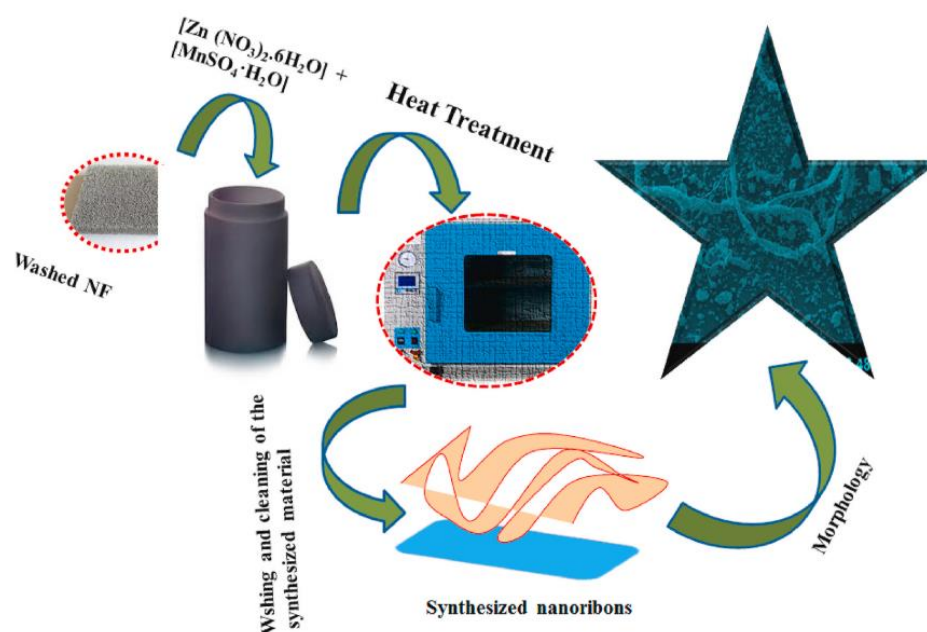


Figure 2.5: Stepwise hydrothermal synthesis procedure (Rashid et al., 2021).

Microwave-assisted hydrothermal method is another process to prepare Mn-doped ZnO nanopowders at different doping ratio of Mn in ZnO (1, 5 and 10 at%). A schematic diagram of microwave-assisted hydrothermal synthesis of nanomaterial is shown in Figure 2.6. Manganese (II) acetate tetrahydrate was served as Mn cation source, zinc acetate dihydrate was served as the Zn cation source while sodium hydroxide (NaOH) was used as hydroxide anion source and forming a homogenous equimolar solution. Next, the solution is slowly added with NaOH aqueous solution until 13.96 pH to produce a milky solution. A temperature-control microwave synthesis system was used to irradiate the solution at 95 °C for 10 min, 20 min and 30 min. After that, the solution

was cooled to room temperature naturally and the filtered. Precipitate collected were washed with deionized water and ethanol for several minutes. Drying of precipitate was carried out in an oven at 60 °C for 24 h. The powder was then calcined in air at 500 °C for 2 h producing flower-like and rod-like morphologies (Aksoy and Caglar, 2019).

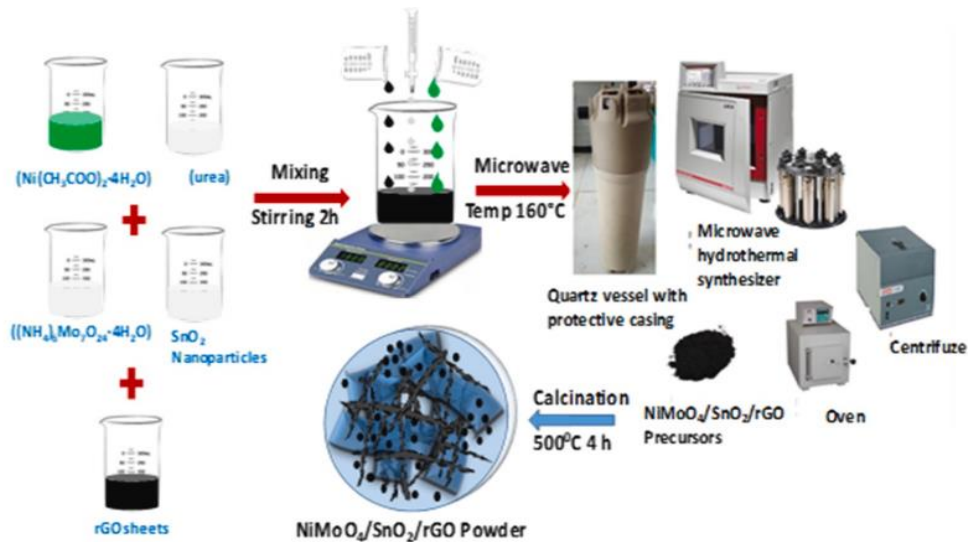


Figure 2.6: Schematic diagram of microwave-assisted hydrothermal method (Naresh et al., 2021).

2.2 Physical Characterization of Manganese Doped Zinc Oxide Nanoparticles

Diverse characterize methods can be used to identify the properties of manganese (Mn) doped ZnO nanoparticles such as X-ray Diffraction (XRD), Scanning Electron Microscopy (SEM), Transmission Electron Microscopy (TEM) and Energy-Dispersive X-ray Spectroscopy (EDX). Those techniques are used in this work to identify the phase, structure, crystallinity and surface morphology of the manganese (Mn) doped zinc oxide (ZnO) nanoparticles.

2.2.1 Phase and Structural Analysis

XRD is a rapid and versatile non-destructive technique used to characterize the crystallographic structure, phases identification, preferred crystal orientations and other

structural parameters of the crystalline material. XRD can be employed to analyse fluids, powders and crystals. It also gives detailed information of material such as average grain size, degree of crystallinity, strain, and crystal defects (Bunaciu et al., 2015).

In the XRD analysis, electrons are emitted when current passed through the tungsten filament and the accelerated electron move towards and strike the anode forming X-ray emission in the cathode ray tube. Then the X-ray is filtered to create monochromatic electromagnetic radiation and passed through collimator to concentrate the radiation. Crystals have regular atomic arrays. The X-ray radiation is focused to a specimen. XRD relies on ability of crystalline material to elastically scatter monochromatic beam of X-rays and producing diffraction pattern when there is constructive interference of scattered X-rays from each set of lattice planes in the specimen at certain angles (Epp, 2016). Bragg's law is the fundamental for XRD and describe the condition for constructive interference.

Since usual interplanar spacing in the crystalline materials can be determined from XRD, it can be used for determination of crystal domain size and structure. XRD pattern is considered as the fingerprint of periodic atomic arrangement for each material, hence by referring the diffraction pattern to ICDD database which is a database of the known XRD pattern, phase identification can be performed (Nasrollahzadeh et al., 2019).

Structural behaviour of the hydrothermal synthesized $Zn_{1-x}Mn_xO$ nanoparticles with varying dopants concentration levels, where $x = 0.01, 0.02, 0.03, 0.04$ and 0.05 heated at $100\text{ }^\circ\text{C}$ for 12 h and calcined at $500\text{ }^\circ\text{C}$ were studied by using XRD technique (Senol et al., 2020). From the XRD spectra in Figure 2.7, no further peak which represent secondary phase related to Mn and their compounds. The XRD pattern of undoped and Mn-doped ZnO nanoparticles up to concentration of 15% as shown in Figure 2.7 and Figure 2.8 can be observed that the diffraction peaks are well corresponded to the JCPDS

36-1451 data of wurtzite ZnO (hexagonal crystal system, P63 mc space group) (Abrinaei and Molahasani, 2018).

The diffraction peaks seen in the Figure 2.7 and Figure 2.8 for $Zn_{1-x}Mn_xO$ in both works are attributes to the reflections from the planes of polycrystalline ZnO at (100), (002), (101), (102), (110), (103), (200), (112), (201), and (202), indicating the Mn ions have successfully introduced into the ZnO lattice site without changing the lattice structure. The sharp and narrow peaks represented the good crystallinity of hydrothermal synthesized Mn-doped ZnO nanoparticles.

It is also found that the peak position for Mn-doped ZnO nanoparticles fabricated through hydrothermal method experienced a slightly shift compared to undoped ZnO as shown in diffraction pattern depicted in Figure 2.8 and Figure 2.9. A shift of peak positions to lower angle when dopant increase may due to increased lattice distance when Mn^{2+} ions having larger ionic radius of 0.80 Å substitutionally replaced Zn^{2+} ions having a smaller radius of 0.74 Å (Xin et al., 2014, Bordbar et al., 2015, Abrinaei and Molahasani, 2018, Aksoy and Caglar, 2019). Correspondingly, the lattice constant increases slightly in the Mn-doped ZnO in comparison with the undoped ZnO. The average crystallite size of Mn-doped ZnO calculated from Scherrer formula is in the range of 20-33nm. Furthermore, the diffraction peak positions might not be significantly affected by the increase of annealing temperature but the intensity of the diffraction peaks experiences markedly reduction.

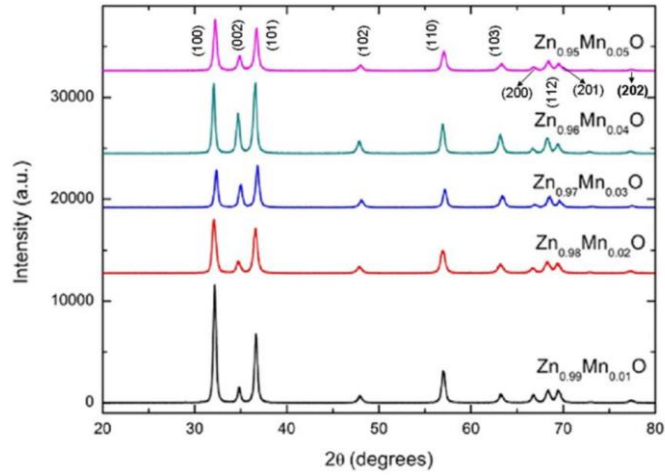


Figure 2.7: XRD patterns of hydrothermal synthesized $Zn_{1-x}Mn_xO$ nanoparticles ($x= 0.01, 0.02, 0.03, 0.04$ and 0.05) (Senol et al., 2020)

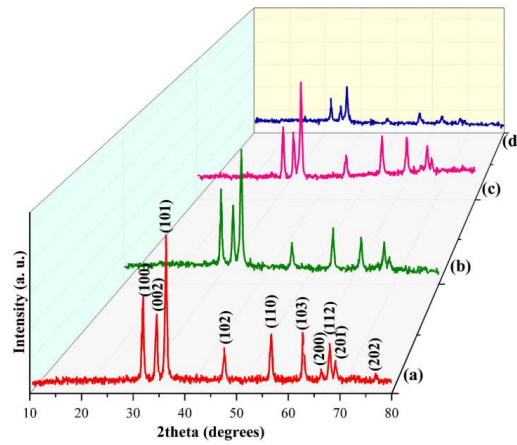


Figure 2.8: 3D plot of XRD spectra for hydrothermal synthesized undoped ZnO nanoparticles and Mn-doped ZnO nanoparticles (2% 5% 15% Mn/ZnO ratio) (Abrinaei and Molahasani, 2018).

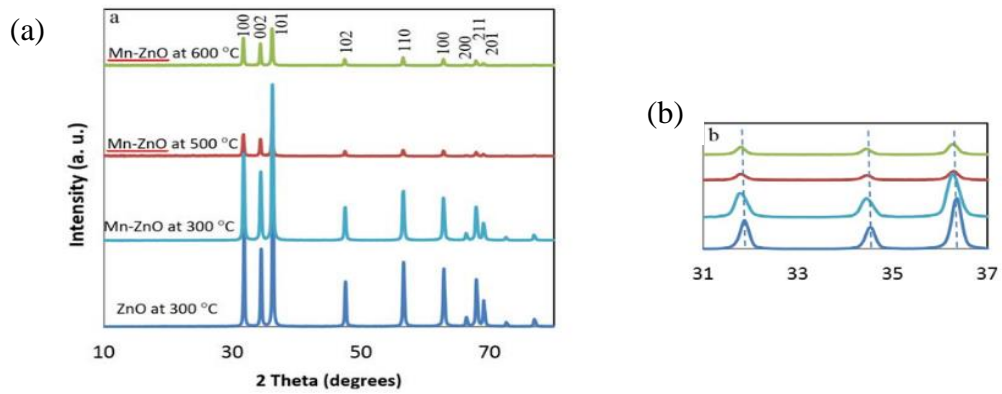


Figure 2.9: XRD pattern of undoped ZnO and Mn-doped ZnO with annealing temperature at 300, 500 and 600°C, (b) (100), (002) and (101) peak position shifting (Bordbar et al., 2015).

2.2.2 Morphological and Elemental with Chemical Composition Analysis

SEM is rapid and versatile instrument used for surface imaging and morphological analysis of solid specimens with tiny features. It utilized a focused beam of high-energy electrons to scan at the surface of a specimen in a raster fashion. The fast-moving electrons dissipated their energy during electron-sample interaction and emit backscattered and secondary electron which then converted into signal to create the image of specimen. Secondary electrons are useful for imaging which provide topographic information while backscattered electron give rise to images presenting a compositional contrast.

For field emission scanning electron microscope (FESEM), electrons are generated by strong electrical field emission source, and accelerated by the high electrical field gradient (Semnani, 2017). SEM photograph created from FESEM is clearer and less electrostatically distorted. it is referred to a field transmitter, which is FESEM that can produce greater photographs. SEM offers magnification ranging from 20X to about 30000X, high level of resolution (about 10nm) and a large depth of field. SEM gather information from different detectors such as morphological characteristics like size and shape, topography, surface composition. Purity, dispersion degree, homogeneity of nanomaterials can also be determined from SEM analysis (Patravale et al., 2012).

The SEM images of different Mn dopant ratios in $Zn_{1-x}Mn_xO$ nanoparticles ($x = 0.01, 0.02, 0.03, 0.04, \text{ and } 0.05$) are displayed in Figure 2.10. All SEM images demonstrates random agglomerated grains with pores. The nanoparticles Zn-doped nanoparticles produced with hydrothermal synthesis also have intertwined and tight structure. It can be seen that the size of nanoparticles varied from each other (Senol et al., 2019, Senol et al., 2020).

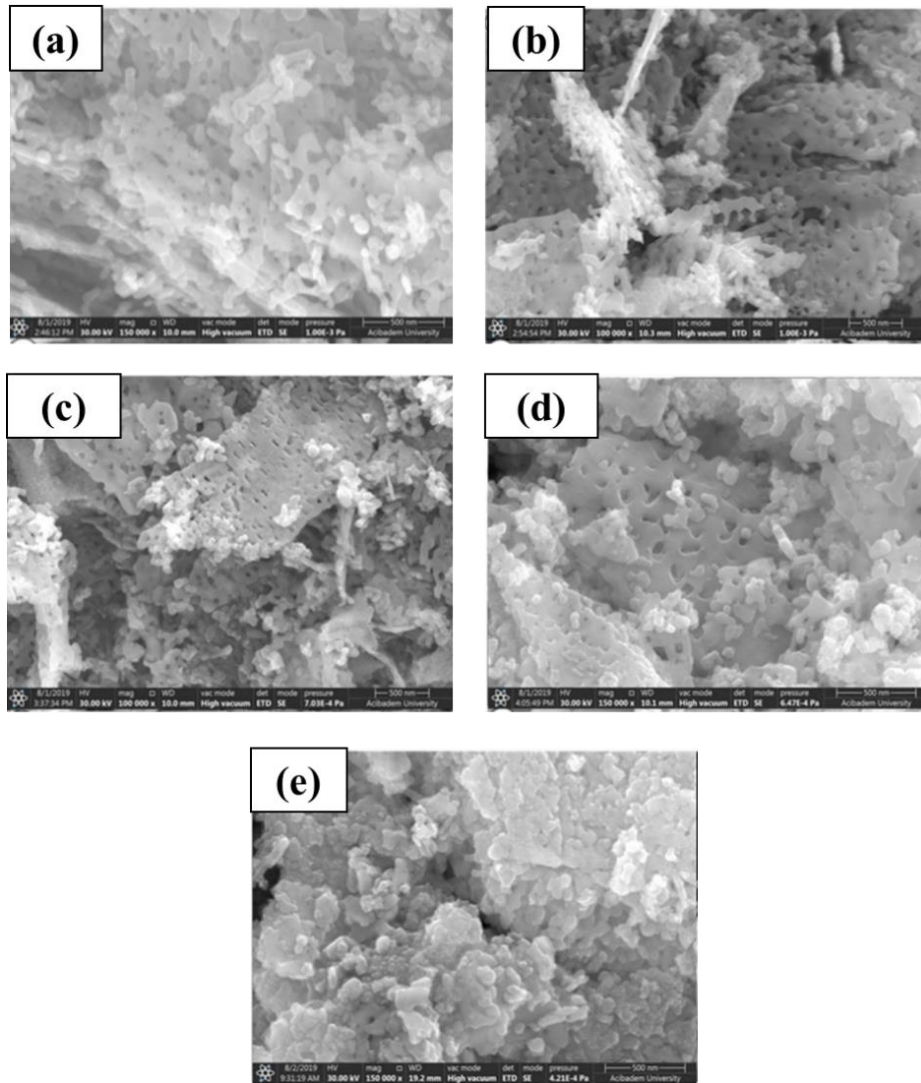


Figure 2.10: SEM images of ZnO nanoparticles with (a) 1 at%, (b) 2 at%, (c) 3 at%, (d) 4 at% and (e) 5 at% Mn doped (Senol et al., 2020).

Figure 2.11 displays the morphology of pure ZnO and doped ZnO nanocrystal at different Mn/ZnO ratio of 2 %, 5 %, and 15 % have spherical pattern with uniform and homogeneous particle size distribution. From FESEM images, the particles sizes increased from 20 to 38 nm with the increasing concentration of Mn. This increase is corresponding to the XRD result of increase in lattice parameter when doping content rises (Abrinaei and Molahasani, 2018).

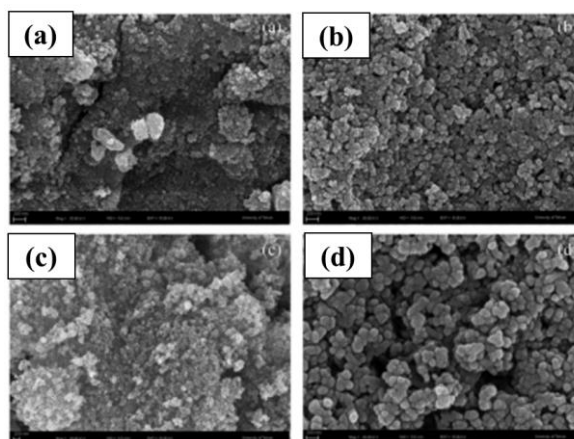


Figure 2.11: FESEM image of (a) undoped ZnO nanoparticles and Mn-doped ZnO nanoparticles with (b) 2%, (c) 5% and (d) 15% of Mn/ZnO ratios (Abrinaei and Molahasani, 2018).

The SEM micrographs of $Zn_{1-x}Mn_xO_3$ of different molar ratio grown on nickel foam via hydrothermal method is shown in Figure 2.12. The scanning electron microscopy was done for the morphological features of the synthesized samples. For doping concentrations with $x = 0, 0.25, 0.75$ and 1 exhibit morphologies of ribbon-like structure and agglomerate grains with unclear boundary. Meanwhile, Figure 2.13 demonstrate the SEM micrographs of $Zn_{0.50}Mn_{0.50}O_3$ at various magnifications. The interconnection of $Zn_{0.50}Mn_{0.50}O_3$ is fully evident, displaying well-defined boundary with crosslinking network nanostructure (Rashid et al., 2021).

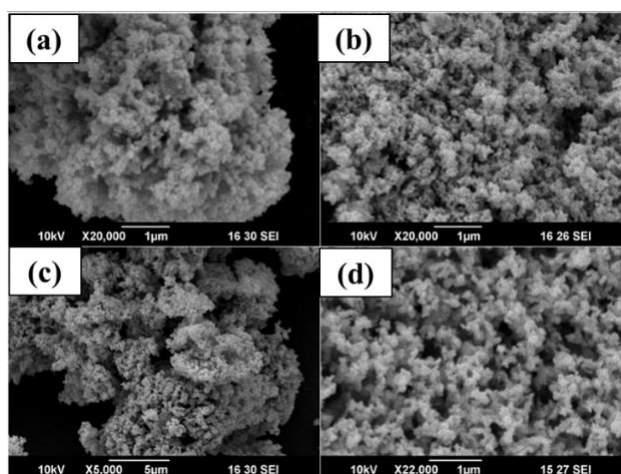


Figure 2.12: SEM micrographs of (a) ZnO, (b) $Zn_{0.75}Mn_{0.25}O_3$, (c) $Zn_{0.25}Mn_{0.75}O_3$, (d) MnO_2 , respectively (Rashid et al., 2021).

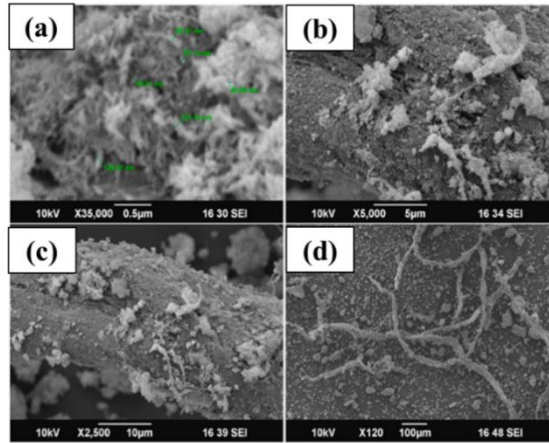


Figure 2.13: SEM micrographs of $Zn_{0.50}Mn_{0.50}O_3$ at various magnifications (a)35000X, (b)5 000X, (c) 2500X, and (d) 120X (Rashid et al., 2021).

Energy-dispersive X-ray spectrometry (EDX), or also known as EDS is a standard characterization method employed for elemental or chemical compositional analysis of nanomaterials. This analytical technique is usually used in conjunction with SEM to determine the relationship between composition, microstructure and elemental spectra. EDX is relies on the characteristic X-ray generated from the interaction of the charged particles stream with high energy like electron or protons or an X-ray beam with the sample. Excitation of inner shell electron happened in the specimen surface atoms when high-energy electron beam bombarded with the sample and ejected inner shell electrons. The transition of outer shell electrons filling the hole left behind in the inner shell emitting an X-ray (Lewis et al., 2012). EDX can detect the amount and energy of the emitted X-rays to obtain the elemental composition of the material and to gather detailed information of the samples (Wei et al., 2021).

EDX spectrums of $Zn_{1-x}Mn_xO$ nanoparticles with different Mn concentration rate of $x = 1, 3$ and 5% are shown in Figure 2.14. Zn, Mn and O peaks are observed in the EDX spectrums, indicating the Mn ions were favorably integrated into the ZnO crystalline structure. From the EDX analysis, the Zn and Mn content is compatible with the sample elemental composition as revealed by the atomic ratios (Senol et al., 2019).